HHS Public Access

Author manuscript

New J Chem. Author manuscript; available in PMC 2017 March 01.

Published in final edited form as:

New J Chem. 2016 March 1; 40(3): 2028–2035. doi:10.1039/C5NJ02108A.

Aggregate-based sub-CMC Solubilization of *n*-Alkanes by Monorhamnolipid Biosurfactant

Hua Zhong[1,2,3,*], **Xin Yang**[1,2], **Fei Tan**[1,2], **Mark L Brusseau**[3], **Lei Yang**[1,2], **Zhifeng Liu**[1,2], **Guangming Zeng**[1,2], and **Xingzhong Yuan**[1,2]

[1]College of Environmental Science and Engineering, Hunan University, Changsha 410082, China

[2]Key Laboratory of Environmental Biology and Pollution Control (Hunan University), Ministry of Education, Changsha, 410082, China

[3]Department of Soil, Water and Environmental Science, University of Arizona, Tucson, Arizona 85721, USA

Abstract

Solubilization of *n*-decane, dodecane, tetradecane and hexadecane by monorhamnolipid biosurfactant (monoRL) at concentrations near the critical micelle concentration (CMC) was investigated. The apparent solubility of all the four alkanes increases linearly with increasing monoRL concentration either below or above CMC. The capacity of solubilization presented by the molar solubilization ratio (MSR), however, is stronger at monoRL concentrations below CMC than above CMC. The MSR decreases following the order dodecane > decane > tetradecane > hexadecane at monoRL concentration below CMC. Formation of aggregates at sub-CMC monoRL concentrations was demonstrated by dynamic light scattering (DLS) and cryo-transmission electron microscopy examination. DLS-based size (d) and zeta potential of the aggregates decrease with increasing monoRL concentration. The surface excess (Γ) of monoRL calculated based on alkane solubility and aggregate size data increases rapidly with increasing bulk monoRL concentration, and then asymptotically approaches the maximum surface excess (Γ_{max}). Relation between Γ and d indicates that the excess of monoRL molecules at the aggregate surface greatly impacts the surface curvature. The results demonstrate formation of aggregates for alkane solubilization at monoRL concentrations below CMC, indicating the potential of employing low-concentration rhamnolipid for enhanced solubilization of hydrophobic organic compounds.

Keywords

biosurfactant; monorhamnolipid; *n*-alkane; critical micelle concentration; solubilization; aggregation

[*]Corresponding author at: Department of Soil, Water and Environmental Science, University of Arizona, 1177 E 4th St., Tucson, AZ 85721, U.S.A. Tel.: +01-520-626-4191; zhonghua@hnu.edu.cn; zhonghua@email.arizona.edu. .
Lei Yang: wlwyanglei@126.com
Fei Tan: tanfei_2013@163.com
Zhifeng Liu: lzf18182002@163.com
Guangming Zeng: zgming@hnu.edu.cn
Xingzhong Yuan: yxz@hnu.edu.cn

1. Introduction

Biosurfactants are amphiphilic molecules produced by microbes. They have the properties of typical surfactants, such as lowering interfacial tension, wetting surface, foaming, and causing solubilization or emulsification of hydrophobic organic compounds (HOCs). Due to their advantages over synthetic surfactants, e.g. low toxicity,[1] high degradability and environmental compatibility,[1] and high efficiency,[2,3] biosurfactants have received increased use for many applications in areas such as chemical manufacturing, pharmaceuticals, contamination remediation, etc.[4] Solubilization of organic compounds is one of the key functions for these applications of biosurfactants. For example, biosurfactant-enhanced aquifer remediation for removal of nonaqueous-phase-liquid HOCs is primarily based on the mechanism of solubilization.[5, 6]

Solubilization of HOCs by surfactants has been studied extensively at high surfactant concentrations, i.e. higher than critical micelle concentration (CMC).[7-14] Micelles are considered to be of spherical shape with three zones for solubilization: the core, the corona, and the core-corona interface.[15, 16] It is typically assumed that solubilization enhancement of hydrophobic compounds only occurs at surfactant concentrations higher than CMC.[11, 16, 17]

The results of some studies, however, showed that surfactants also solubilize HOCs at sub-CMC concentrations. For example, result of our prior study showed that synthetic surfactants SDBS and Triton X-100 enhanced solubilization of hexadecane at concentrations below CMC based on an aggregate formation mechanism.[18] There is evidence of similar behavior for biosurfactants, with Zhang and Miller reporting that solubility of octadecane was enhanced by rhamnolipid biosurfactant at sub-CMC concentrations. It is interesting to note that the enhancement was much more significant at concentrations below the CMC than at concentrations above CMC.[8] It was assumed that this sub-CMC enhancement of octadecane solubilization was due to the decrease of water-octadecane interfacial tension.[8] In our prior study of hexadecane solubilization by a monorhamnolipid, similar results were also observed.[19] Research is needed to delineate the mechanisms contributing to the sub-CMC solubilization capability observed for biosurfactants. This information is also relevant for commercial application of biosurfactants in trems of cost effectiveness

Solubilization of *n*-alkanes by rhamnolipid biosurfactant at concentrations near CMC was investigated in this study, with a focus on solubilization behavior at concentrations lower than CMC. Monorhamnolipid (monoRL), a group of rhamnolipid species with one rhamnose ring and two alkyl chains (Figure 1), was used in this study. It is considered an anionic surfactant under the experiment conditions in this study due to the carboxyl group in the molecule (pK_a=5.6 under ambient temperature [20]). Four linear alkanes (i.e. *n*-decane, *n*-dodecane, *n*-tetradecane and *n*-hexadecane) with different chain lengths were selected to represent HOCs. In addition to *n*-alkanes solubility, characterizations of alkane-monoRL aggregates, such as measurement of aggregate size and zeta potential and cryo-TEM-based observation of aggregate morphology, were implemented. Finally, surfactant interface partition theory, an assumption of spherical aggregates, and surfactant mass balance was used to interpret the sub-CMC solubilization of the alkanes by the rhamnolipid.

2. Theoretical Background

Based on the classical model regarding the structure of alkane-surfactant aggregates formed in solution for alkane solubilization, the aggregates are assumed to be spherical, comprising the alkane residing in the core zone and a layer of surfactant molecules on surface with their alkyl chains intermingling in the core with the alkane molecules. Rhamnolipid molecules reside in bulk solution (C_w) or in the aggregates, for which the partition can be described using Gibbs and Langmuir adsorption equations [21-23]. In addition, the total mass of rhamnolipid in bulk solution and as aggregates is equal to the mass of rhamnolipid initially added. Based on these assumptions, partition of rhamnolipid between bulk solution and aggregate phase at solubilization equilibrium can be calculated using measures of interfacial tension and aggregate size. The theoretical details can be found in ref. 18.

3. Materials and Methods

3.1 Materials

The monoRL biosurfactant (purity > 99.9%) was purchased from Zijin Biological Technology Co., Ltd. (Huzhou, China). Constituent characterization of the monoRL is described by Zhong et al.[24]. The monoRL comprises five species of Rha-C_{10}-C_8, Rha-C_{10}-$C_{10:1}$, Rha-C_{10}-C_{10}, Rha-C_{10}-$C_{12:1}$ and Rha-C_{10}-C_{12}, where the abbreviation Rha-C_x-$C_{y:z}$ represents the individual component with x and y as the carbon atom number of each alkyl chain in the lipid moieties, and z as the number of unsaturated bonds in lipid moieties. Rha-C_{10}-C_{10} at the relative molar abundance of 75.5% is the major component.

The *n*-alkanes (*n*-decane, *n*-dodecane, *n*-tetradecane and *n*-hexadecane) (purity > 99%) were purchased from Sigma-Aldrich (St. Louis, Mo., U.S.). The selected properties of the *n*-alkanes are listed in Table 1 and molecule structure is shown in Figure 1. *n*-Octane (purity > 95.0%) and HPLC grade ethanol were purchased from Damao Chemical Reagent Co. Ltd. (Tianjin, China). All other chemicals were of analytical grade and used as received. Ultra-pure water with electrical resistivity of 18.2 MΩ·cm produced by UPT- II −40 (Ulupure, Chengdu, China) was used throughout the experiment. Phosphate buffer (PBS, 1.24 g/L KH_2PO_4 and 1.35 g/L $K_2HPO_4{\cdot}3H_2O$, pH 6.8) was used as the background electrolyte solution for monoRL solubilization. It provides a stable concentration of counterions, which is important for application of the Gibbs adsorption equation for monoRL with ionic nature. In this PBS buffer, the degree of dissociation for the monoRL is 94% based on pK_a of 5.6 [20]. Such a high degree of dissociation also supports the assumption that the monoRL is anionic and resides only in bulk solution or at interface in this study.

3.2 Surface and interfacial tension measurement

Interfacial tension between alkane and monoRL solutions with designated monoRL concentrations was measured at 30°C with a tensiometer (JZ-200A, Chengde, China) using the Du Noüy Ring method.[29] In brief, 15 mL of monoRL solution in PBS was prepared in a 50 mL glass beaker. 15 mL of alkane was then carefully added to the top of the monoRL solutions without disturbing the solution. Before the interfacial tension was measured, the beaker was kept at 30°C for half an hour to allow partitioning of monoRL to the water-

alkane interface to reach equilibrium. The measurements were reproducible, with the difference of duplicate measurements within ±0.2 mN/m. For reference purposes, the surface tension (interfacial tension between air and solution) of the monoRL solution was also measured.

3.3 Solubilization of *n*-alkane by monoRL

For each *n*-alkane-monoRL combination, 50 μL of alkane was pipetted and spread on the bottom of a 25-mL glass flask. 10 mL of monoRL solution in PBS was then added to the flask and incubated on a reciprocal shaker at 30°C, 120 rpm for 24 h to allow the solubilization to reach equilibrium (result of a preliminary test showed that alkane solubility did not change after 24 h). The flasks were allowed to stand for 2 h for phases to separate, then 4 ml of aqueous solution saturated with only pseudo-solubilized hexadecane was separated using the method described by Zhong et al.[19] 1 mL of the collected samples was removed for alkane concentration measurement, and another 2 mL was used for measurement of size and zeta potential of the aggregates. The alkane concentration was measured using gas chromatography (Agilent GC 6890N) following the procedures described by Zhong et al.[19]. A control containing 10 mL monoRL solution and no alkane was used to quantify loss of monoRL due to adsorption to the inner wall of the flasks.

The size and zeta potential of aggregate particles were measured using a ZEN3600 Zetasizer Nano (Malvern Instruments, U.K.). The particle size was determined based on the method of dynamic light scattering (DLS) at 633 nm with He-Ne laser working on a 4 mV power. 1 mL of sample was loaded to the DTS-0012 cell and maintained at 30°C. The scattered light was collected by receptor at angle of 173° from light path. The size of the aggregates was expressed in terms of hydrodynamic diameter, which was calculated by using the software associated with the instrument. To obtain the zeta potential of the aggregates, approximately 1 mL of sample was loaded to the DTS1060 folded capillary cell and the electrophoretic mobility of the aggregate particles was measured at 30°C under automatic voltage using laser Doppler velocimetry with M3-PALS technique to avoid electroosmosis. The measured data was converted into corresponding zeta potential applying the Helmholtz-Smoluchowski equation.[30]

3.4 Cryo-Transmission Electron Microscopy (cryo-TEM) observation of hexadecane-monoRL aggregates

A 4 μL drop of solubilized hexadecane solution was placed on a copper grid, and then sent to a FEI Vitrobot sample plunger. The excess sample was removed with filter paper. The grid was then immediately plunged into a bath of liquid ethane and transferred to a bath of liquid nitrogen. The samples were stored in a GATAN model cryo-transfer unit in liquid nitrogen. The morphology of surfactant-hexadecane aggregates was viewed with a Tecnai F20 cryo-transmission electron microscope (FEI, Hillsboro, Oregon) at 120 kV.

4. Results and discussion

4.1 CMC and interfacial partitioning parameters

The dependence of air-PBS and *n*-alkane/PBS interfacial tension on monoRL concentration is presented in Fig. 2a. CMCs calculated using the method described by Zhong et al.[31] are presented in Table 1. The CMCs of monoRL obtained using surface tension or interfacial tension measurements are similar to each other, showing that the non-aqueous phase (air or alkanes) has little impact on CMC. An average CMC of 158±9 μM is obtained.

The interfacial tension data at sub-CMC monoRL concentration are well fitted by equation (3) in ref.18 (Fig. 2b), and K, Γ_{max}, and A_m obtained are summarized in Table 1. K decreases following the order dodecane > decane > tetradecane > hexadecane. Alkyl chain length of the monoRL is similar to that of dodecane and decane (Figure 1), which may be favorable for ordered alignment of monoRL-alkane molecules at the interface and hence lower Gibbs energy, resulting in a stronger partitioning of monoRL at the interface for dodecane and decane. However, Γ_{max} is larger (A_m is smaller) for tetradecane and hexadecane, showing that when the adsorption is saturated the monoRL molecules are more compacted at the interface for long-chain alkanes.

4.2 Solubilization of *n*-alkanes by monoRL

Apparent solubility of alkanes as a function of monoRL concentration is shown in Fig. 3. For all four alkanes, the solubility is enhanced at monoRL concentrations below CMC. The apparent solubility of each alkane increased linearly with monoRL concentration at different rates below and above CMC.

The solubilization capacity of a surfactant for a HOC is presented by the molar solubilization ratio (MSR), which is defined as the increase of solubilized HOC concentration (mol/L) per unit increase of surfactant concentration (mol/L) in the solution, or the slope of the linear solubilization curve.[32] The MSR for the four alkanes are listed in Table 2. MSR for all of the four alkanes are significantly higher at monoRL concentration below CMC than above CMC. Similar results were observed for octadecane solubilization by monoRL,[8] and hexadecane solubilization by SDBS (also an anionic surfactant)[18].

These observations indicate a difference in modes of alkane solubilization below and above CMC. The MSR decreases following the order dodecane > decane > tetradecane > hexadecane at monoRL concentrations below CMC (Table 2), which is the same as the order for K. This indicates a relationship between alkane solubilization and interfacial partitioning of monoRL. It is worth noting that the MSR for hexadecane solubilization by the monoRL at sub-CMC concentrations (2.55) is larger than that for SDBS (0.84) and Triton X-100 (1.90)[18], indicating higher solubilization efficiency of biosurfactant monoRL over synthetic surfactants. This is probably due to the presence of the double alkyl chains in the monoRL molecule.

4.3 Size and zeta potential of aggregates

The formation of aggregates was detected by aggregate size measurement using the DLS method. A single peak is observed for the number-based particle size distribution profile, indicating formation of one consistent size of aggregate (Fig.4). The aggregates are observed directly with cryo-TEM, and the spherical aggregate morphology is confirmed (Fig. 5). Also, the size of the aggregates as measured by cryo-TEM is similar to the DLS-measured size. The aggregates shown by cryo-TEM do not appear when hexadecane is equilibrated with aqueous solution without monoRL (data not shown).

For all four alkanes, the DLS particle size first decreases rapidly with increase of total rhamnolipid concentration, C_0, and then stabilizes with increase of C_0 to above CMC (Fig. 6). By comparing between alkanes, it is observed that the aggregates size at monoRL concentration of CMC decreases following the order decane ≈ dodecane > tetradecane > hexadecane. This order is in contrast to the order of Γ_{max} for these four alkanes, which is decane ≈ dodecane < tetradecane < hexadecane (Table 1).

Zeta potentials of the aggregates are shown in Fig. 7. The aggregates are negatively charged. The change of zeta potential with increase of C_0 exhibits a similar trend for all four alkanes,. It decreases rapidly with increase of C_0 to CMC, and then stabilizes or decreases slowly with further increase of monoRL concentration.

4.4 Partitioning of monoRL and its relation with aggregation

No emulsion of alkanes in the presence of monoRL was observed in the experiments. Adsorption of the monoRL to the inner wall of the flask was minimal (data not shown). Because very limited volume of alkanes (50 μL, see Materials and Methods section) was used, partition of monoRL to the alkane phase, or to the interface between the floating mass of alkane and the aqueous phase (less than 1 cm^2 in contrast to the magnitude of $10\sim10^3$ cm^2 for the total surface area of the aggregates according to calculation below), was minimal. Therefore, the monoRL can be assumed to reside either in bulk aqueous solution or in the aggregates. Due to the extremely low water solubility and high octanol-water partition coefficient (K_{ow}) of these four alkanes (Table 1), the amount of freely-dissolved alkane in bulk aqueous phase is minimal and all the solubilized alkane is assumed to be associated with the aggregates. Hence, based on the spherical aggregate assumption, the aggregate surface excess, Γ, and the bulk concentration, C_w, of monoRL monomer were calculated by applying equation (2) and (5) in ref.18 using Γ_{max} and K previously obtained.

For all four alkanes, a linear relationship between the apparent solubility of alkane, C_{alk}, and C_w is observed with increase of C_w to CMC (Fig. 8a). This is similar to the relationship between C_{alk} and C_0 which is the total monoRL concentration in solution (Fig. 3). By comparing the slopes of the C_{alk}-C_0 profiles at C_0 below CMC with those of the C_{alk}-C_w profiles (5.7 versus 7.5 for decane, 8.3 versus 10.8 for dodecane, 3.3 versus 5.3 for tetradecane, and 2.55 versus 6.3 for hexadecane), the percentage of the aggregate-associated monoRL is calculated to be 24%, 23%, 38%, and 59% of the total for decane, dodecane, tetradecane, and hexadecane, respectively. Note that the aggregate size for hexadecane is significantly smaller than that for the other three alkanes at C_0 lower than CMC. The higher

surface area for smaller particles is responsible for the enhanced partition of monoRL to theaggregates, in spite of the fact that the K and solubilized concentration for hexadecane is the smallest among the four alkanes.

The dependence of monoRL surface excess (Γ) and molecule area (A) versus C_w are presented in Fig. 8b. A rapid increase of Γ and decrease of A with increasing C_w are observed when C_w is low. Further increase of C_w causes asymptotic approach of Γ and A to Γ_{max} and A_m, respectively. More significant change of Γ and A is observed for the long-chain alkanes (tetradecane and hexadecane). Based on equation (2) in ref.18, Γ is more sensitive to change of C_w with a smaller K. The K for four alkanes follows the order of dodecane > decane > tetradecane > hexadecane (Table 1). Thus, the most significant change of Γ and A over the broadest range of C_w occurred for hexadecane.

As shown in Fig. 9, for all four alkanes, aggregate size, d, decreases with the increase of monoRL surface excess in the aggregates, such that d approaches the stabilized minimum aggregate size (d_{min}) as Γ approaches Γ_{max}. This result indicates that the curvature of the aggregate surface increases with increasing surface excess of monoRL molecules. Because monoRL is anionic and 94% of the monoRL molecules dissociates in PBS, the presence of monoRL causes a negative aggregate surface charge. Enhancement in electrostatic repulsion induces unequal rate of approach for polar and hydrophobic moieties between molecules, and therefore an increase in aggregate surface curvature (Fig. 10). Thus, the aggregate size, d, decreases with increasing Γ. Zeta potential is a function of both particle size and surface charge density.[30, 34, 35] Therefore, it is essentially a function of Γ and its change also exhibits an asymptotic decrease pattern at concentrations lower than CMC (see Figure 7).

When monoRL concentration in bulk solution (C_w) is higher than CMC, Γ at the aggregate surface reaches Γ_{max} and the size of aggregates reaches the minimum, giving low efficiency for alkane solubilization. As a result, the MSR at monoRL concentrations above CMC is significantly smaller than that for monoRL concentrations below CMC.

5. Conclusion

The results of this study demonstrated that monorRL biosurfactant at concentrations lower than critical micelle concentration can enhance n-alkanes solubilization. The results also support that such solubilization enhancement is caused by an aggregate formation mechanism. Moreover, the solubilization enhancement at sub-CMC concentrations is more significant for the alkanes with chain length similar to monoRL alkyl chain length. This appears to be the first report delineating the mechanism responsible for the sub-critical micelle concentration solubilization of hydrophobic organic compounds by biosurfactantd, which successfully explains observations of sub-CMC solubilization of alkanes by rhamnolipid in prior studies (i.e. ref. 8 and 19). The study is of importance for better understanding the solubilization behavior of hydrophobic organic compounds by rhamnolipid and for economical application of rhamnolipid biosurfactant in related areas. Future studies should aim at testing sub-critical micelle concentration solubilization behavior of rhamnolipid for other classes of hydrophobic organic compounds, and in other matrices such as porous media.

Acknowledgments

The authors thank the Center for Integrative Imaging (CII) at University of Science and Technology of China for cryo-TEM analysis. This study was funded by the National Natural Science Foundation of China (51378192, 51378190, 51308200 and 21276269), and the Program for Changjiang Scholars and Innovative Research Team in University (IRT-13R17). Additional support was provided by the NIEHS Superfund Research Program (P42 ES04940).

References

1. Fu HY, Zeng GM, Zhong H, Yuan XZ, Huang GH. Biodegradation. 2007; 18:303–310. [PubMed: 17106758]
2. Liu XL, Zeng GM, Tang L, Zhong H, Wang RY, Fu HY, Liu ZF, Huang HL, Zhang JC. Process Biochem. 2008; 43:1300–1303.
3. Zhong H, Liu Y, Liu ZF, Jiang YB, Tan F, Zeng GM, Yuan XZ, Yan M, Niu QY, Liang YS. Int. Biodeter. Biodegr. 2014; 94:152–159.
4. Banat IM, Franzetti A, Gandolfi I, Bestetti G, Martinotti MG, Fracchia L, Smyth TJ, Marchant R. Appl. Microbiol. Biotechnol. 2010; 87:427–444. [PubMed: 20424836]
5. Abriola LM, Drummond CD, Hahn EJ, Hayes KF, Kibbey TCG, Lemke LD, Pennell KD, Petrovskis EA, Ramsburg CA, Rathfelder KM. Environ. Sci. Technol. 2005; 39:1778–1790. [PubMed: 15819238]
6. Childs J, Acosta E, Annable MD, Brooks MC, Enfield CG, Harwell JH, Hasegawa M, Knox RC, Rao PS, Sabatini DA, Shiau B, Szekeres E, Wood AL. J. Contam. Hydrol. 2006; 82:1–22. [PubMed: 16233935]
7. Kile DE, Chiou CT. Environ. Sci. Technol. 1989; 23:832–838.
8. Zhang Y, Miller RM. Appl. Environ. Microb. 1992; 58:3276–3282.
9. Pennell KD, Abriola LM, Weber WJ Jr. Environ. Sci. Technol. 1993; 27:2332–2340.
10. McCray JE, Bai G, Maier RM, Brusseau ML. J. Contam. Hydrol. 2001; 48:45–68. [PubMed: 11291481]
11. Clifford JS, Ioannidis MA, Legge RL. J. Colloid Interface Sci. 2007; 305:361–365. [PubMed: 17081555]
12. Albino JD, Nambi IM. J. Environ. Sci. Heal. A. 2009; 44:1565–1573.
13. Damrongsiri S, Tongcumpou C, Weschayanwiwat P, Sabatini DA. J. Hazard. Mater. 2010; 181:1109–1114. [PubMed: 20579809]
14. Matsuoka K, Yamashita R, Ichinose M, Kondo M, Yoshimura T. Colloids and Surfaces A: Physicochem. Eng. Aspects. 2014; 456:83–91.
15. Patist A, Kanicky JR, Shukla PK, Shah DO. J. Colloid Interface Sci. 2002; 245:1–15. [PubMed: 16290329]
16. Mir MA, Chat OA, Najar MH, Younis M, Dar AA, Rather GM. J. Colloid Interface Sci. 2011; 364:163–169. [PubMed: 21906748]
17. Tehrani-Bagha AR, Holmberg K. Materials. 2013; 6:580–608.
18. Zhong H, Yang L, Zeng G, Brusseau ML, Wang Y, Li Y, Liu Z, Yuan X, Tan F. RSC Advances. 2015; 5:78142–78149. [PubMed: 26925230]
19. Zhong H, Liu Y, Liu ZF, Jiang YB, Tan F, Zeng GM, Yuan XZ, Yan M, Niu QY, Liang YS. Int. Biodeter. Biodegr. 2014; 94:152–159.
20. Ishigami Y, Gama Y, Nagahora H, Yamaguchi M, Nakahara H, Kamata T. Chem. Lett. 1987; 16:763–766.
21. Chen L, Kibbey TC. Langmuir. 2006; 22:6874–6880. [PubMed: 16863233]
22. Peng S, Brusseau ML. Water Resour. Res. 2005; 41:6874–6880.
23. Rosen, MJ. Surfactants and Interfacial Phenomena. 3rd edn. John Wiley & Sons; Hoboken: 2004.
24. Zhong H, Jiang Y, Zeng G, Liu Z, Liu L, Liu Y, Yang X, Lai M, He Y. J. Hazard. Mater. 2015; 285:383–388. [PubMed: 25528238]

25. NCBI. [accessed May 2 7, 2015] PubChem Compound Database; CID=15600, selected properties of n-Decane. http://pubchem.ncbi.nlm.nih.gov/compound/15600
26. NCBI. [accessed May 2 7, 2015] PubChem Compound Database; CID=8182, selected properties of n-Dodecane. http://pubchem.ncbi.nlm.nih.gov/compound/8182
27. NCBI. [accessed Ma y 27, 2015] PubChem Compound Database; CID=12389, selected properties of n -Tetradecane. http://pubchem.ncbi.nlm.nih.gov/compound/12389
28. NCBI. [accessed May 8, 2015] PubChem Compound Database; CID=11006, selected properties of n-Hexadecane. http://pubchem.ncbi.nlm.nih.gov/compound/11006
29. Yuan XZ, Ren FY, Zeng GM, Zhong H, Fu HY, Liu J, Xu XM. Appl. Microbiol. Biot. 2007; 76:1189–1198.
30. Zasoski, RJ. Encyclopedia of Soil Science. Chesworth, W., editor. Springer; Netherlands, Dordrecht: 2008. p. 841-845.
31. Zhong H, Zeng GM, Liu JX, Xu XM, Yuan XZ, Fu HY, Huang GH, Liu ZF, Ding Y. Appl. Microbiol. Biot. 2008; 79:671–677.
32. Edwards DA, Luthy RG, Liu Z. Environ. Sci. Technol. 1991; 25:127–133.
33. Liu W, Kumar J, Tripathy S, Samuelson LA. Langmuir. 2002; 18:9696–9704.
34. Dzombak, DA.; Morel, FMM. Surface Complex Modeling,Hydrous Ferric Oxide. John Wiley & Sons; New York: 1990.
35. Hunter, RJ. Zeta Potential in Colloid Science. Principles and Applications. Academic Press; New York: 1981.

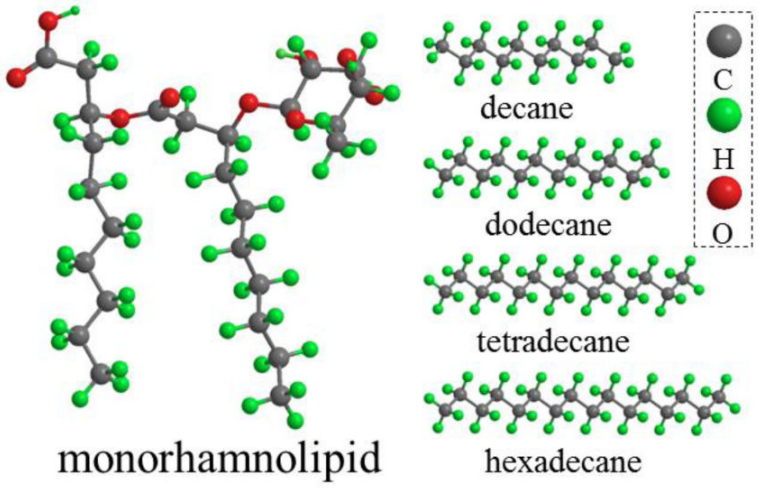

Figure 1.
Molecular structure of monoRL and the four *n*-alkanes.

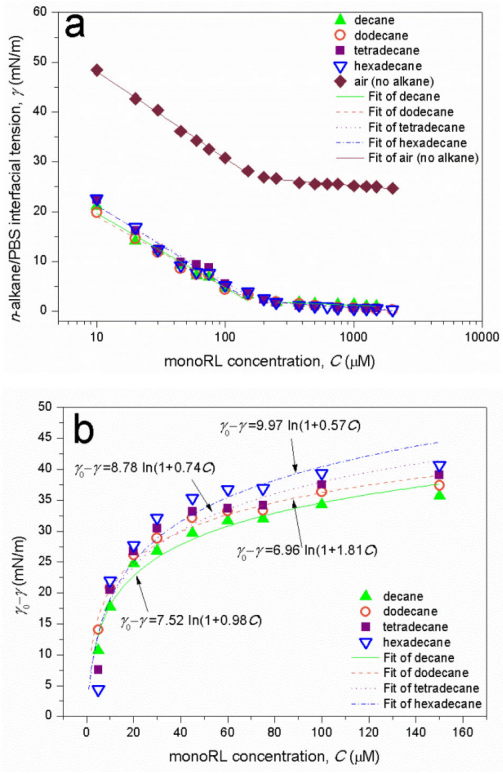

Figure 2.

(a) The air-PBS and *n*-alkanes/PBS interfacial tension as a function of monoRL concentration. (b) Interfacial tension-concentration relation regression at monoRL concentrations below CMC using Szyszkowski equation (Equation (3) in ref.18).

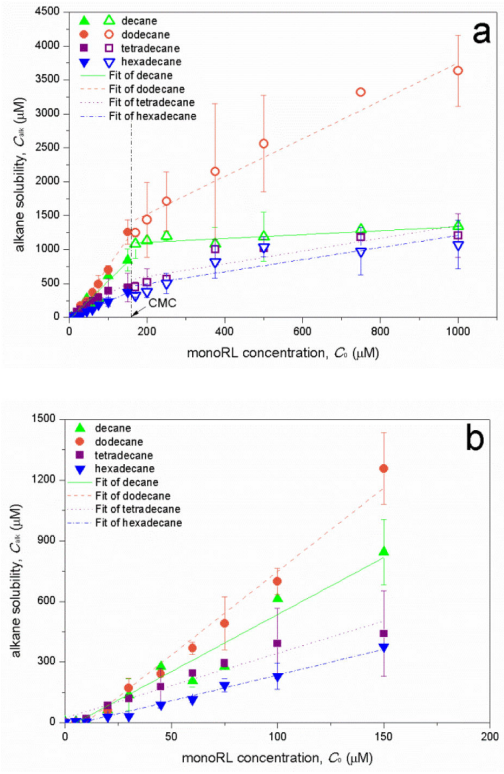

Figure 3.

(a) Apparent *n*-alkanes solubility (C_{alk}) versus monoRL total concentration (C_0). Two sets of regressions represent data for below and above the CMC. (b) Zoom-in for C_{alk}-C_0 relation for C_0 lower than CMC. Error bars show mean ± standard deviation.

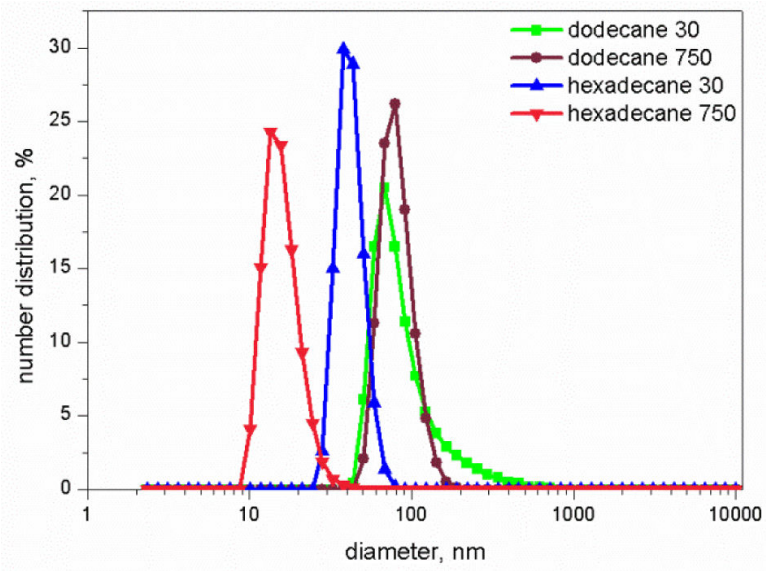

Figure 4.

Number distribution of aggregate particles for solubilization of dodecane and hexadecane by monoRL at concentration of 30 μM and 750 μM.

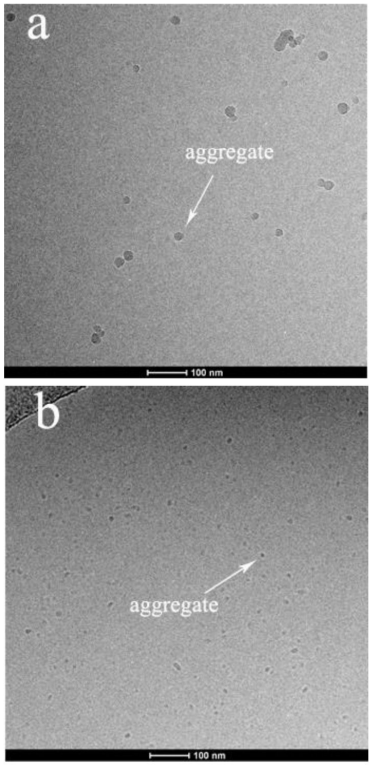

Figure 5.
Cryogenic-transmission electron microscopy (cryo-TEM) images showing aggregates for the solubilization of hexadecane by monoRL at monoRL concentration of 30μM (below CMC) (a) and 750μM (above CMC) (b).

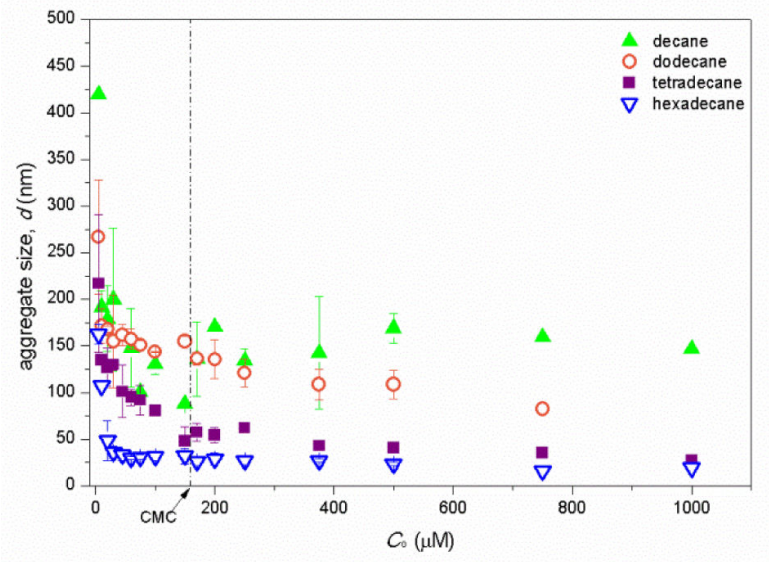

Figure 6.

DLS aggregate size (diameter, *d*) versus the total monoRL concentration (C_0) for the *n*-alkanes solubilization. Error bars show mean ± standard deviation.

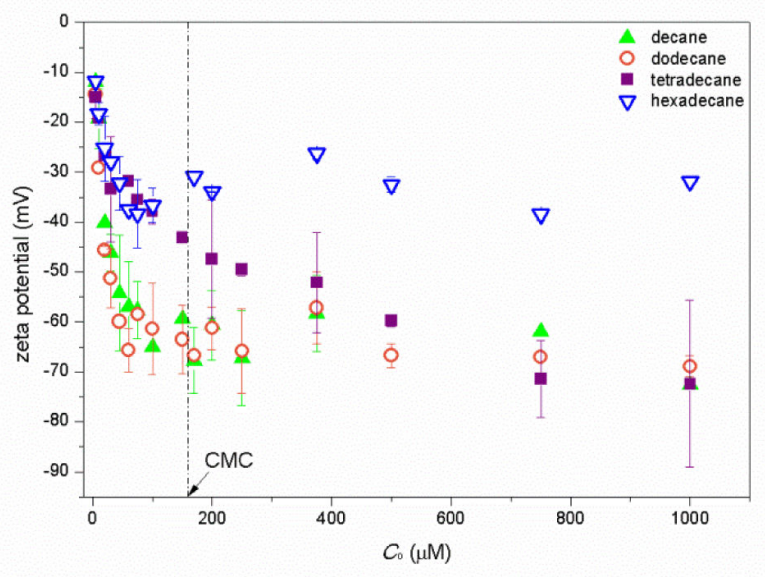

Figure 7.

Zeta potential of aggregates versus the monoRL total concentration (C_0) for the *n*-alkanes solubilization. Error bars show mean ± standard deviation.

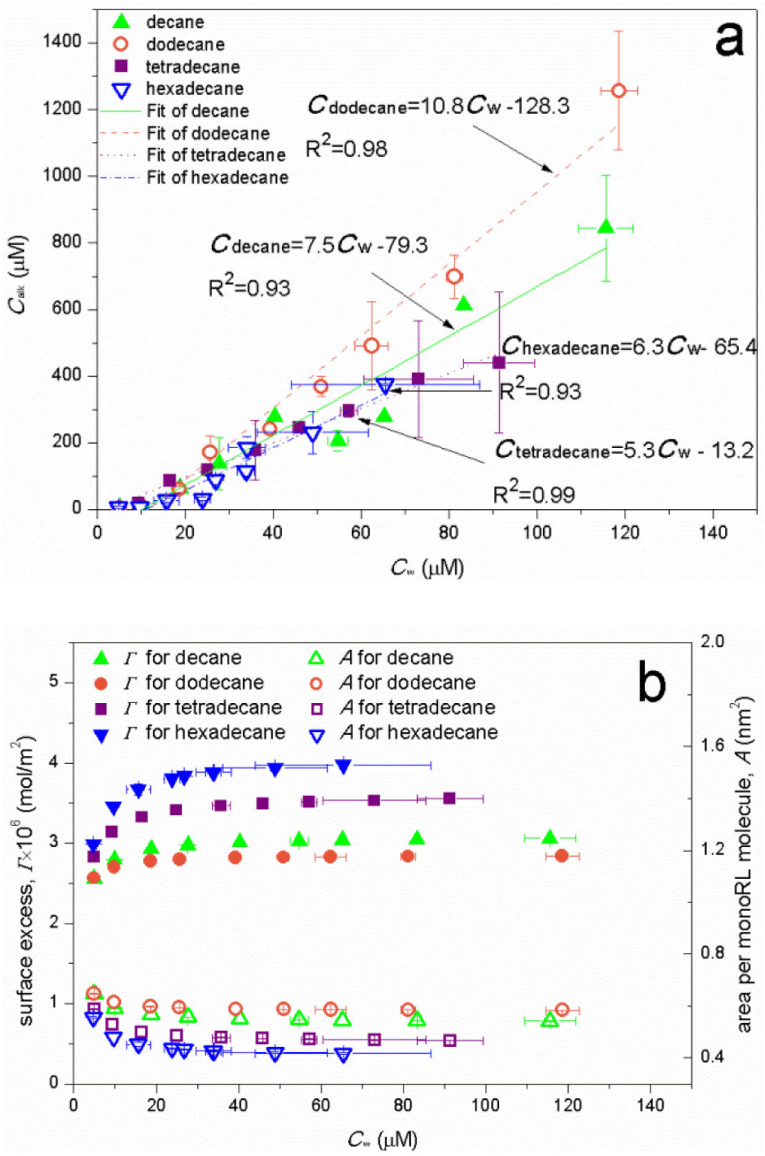

Figure 8.

(a) Apparent solubility of *n*-alkanes (C_{alk}) versus the monoRL bulk concentration (C_w) at C_w below CMC. (b) Surface excess (Γ) and molecule area (A) of monoRL on the aggregates surface versus monoRL bulk concentration (C_w). Error bars show mean ± standard deviation.

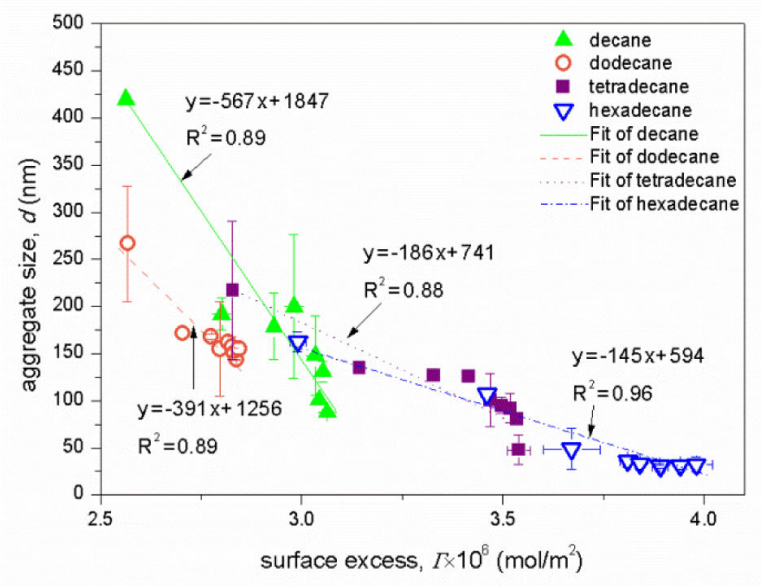

Figure 9.

Aggregates diameter (d) versus surface excess of monoRL (Γ) at monoRL bulk concentration (C_w) below CMC. Error bars show mean ± standard deviation.

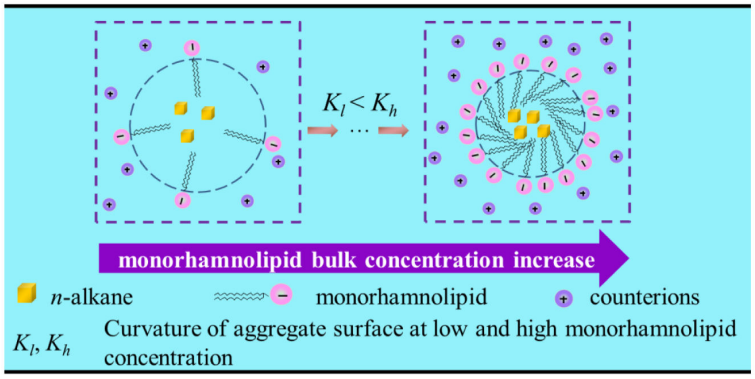

Figure 10.

Schematic diagram of alkane-monoRL aggregate formation at monoRL concentration below CMC.

Table 1

Selected properties of *n*-alkanes and the alkane-PBS interface coefficients of monoRL

***n*-Alkane**	**Formula**	**Molecule weight (g/mol)**	**Water solubility [a] (μM, 25°C)**	**log K_{ow} [b] (25°C)**	**Density [c] (g/cm^3, 25°C)**	***CMC*[d] (μM)**	***K*** **(m^3/mol)**	**Γ_{max} (mol/m^2)**	**A_m (nm^2)**
decane	$C_{10}H_{22}$	142	0.37	5.01	0.73	150	0.98×10^{3}	3.1×10^{-6}	0.54
dodecane	$C_{12}H_{26}$	170	0.02	6.10	0.75	155	1.81×10^{3}	2.9×10^{-6}	0.58
tetradecane	$C_{14}H_{30}$	198	0.01	7.20	0.76	169	0.74×10^{3}	3.6×10^{-6}	0.46
hexadecane	$C_{16}H_{34}$	226	0.0004	8.25	0.77	152	0.57×10^{3}	4.1×10^{-6}	0.41

[a] Solubilities of *n*-alkanes are reported by NCBI (ref. 25-28)

[b] Octanol-water partition coefficient (K_{OW}) values of *n*-alkanes from NCBI (ref. 25-28)

[c] Relative density (water=1) of *n*-alkanes from NCBI (ref. 25-28)

[d] Critical micelle concentration (CMC) for monoRL biosurfactant in the presence of *n*-alkanes obtained by *n*-alkane/PBS interfacial tension measurement (CMC obtained by surface tension measurement in the absence of *n*-alkanes is 166 μM)

Table 2

The molar solubilization ratio (MSR) for alkanes solubilization by monoRL

***n*-Alkane**	**MSR**	
	Below CMC	**Above CMC**
decane	5.73	0.29
dodecane	8.28	2.91
tetradecane	3.27	0.94
hexadecane	2.55	0.89